

A thermodynamically motivated model for ferroelectric ceramics with grain boundary effects

To cite this article: A Arockiarajan *et al* 2010 *Smart Mater. Struct.* **19** 015008

View the [article online](#) for updates and enhancements.

You may also like

- [Domain switching emission from the mixed-mode crack in ferroelectrics by birefringence measurement and phase field modeling](#)

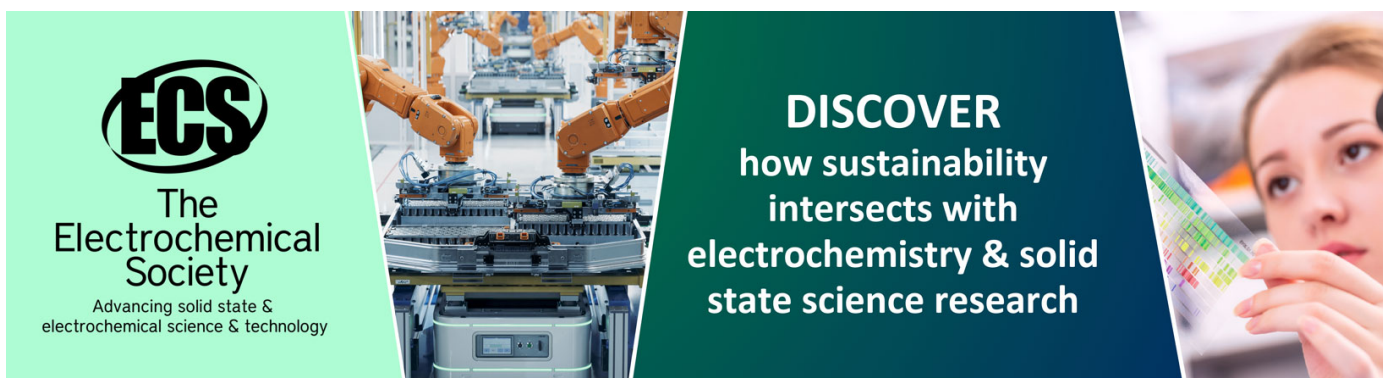
Qun Li, Suxin Pan, Qida Liu et al.

- [Electrical fatigue behaviour in lead zirconate titanate: an experimental and theoretical study](#)

Mainak Bhattacharyya and A Arockiarajan

- [Effect of grain size on the domain structures and electromechanical responses of ferroelectric polycrystal](#)

Xinkai Li and Jie Wang



ECS
The
Electrochemical
Society
Advancing solid state &
electrochemical science & technology

DISCOVER
how sustainability
intersects with
electrochemistry & solid
state science research

A thermodynamically motivated model for ferroelectric ceramics with grain boundary effects

A Arockiarajan¹, S M Sivakumar¹ and C Sansour²

¹ Department of Applied Mechanics, Indian Institute of Technology Madras, Chennai 600 036, India

² School of Civil Engineering, University of Nottingham, Nottingham NG7 2RD, UK

E-mail: aarajan@iitm.ac.in

Received 6 May 2009, in final form 8 October 2009

Published 24 November 2009

Online at stacks.iop.org/SMS/19/015008

Abstract

The aim of this paper is to capture the grain boundary effects taking into consideration the nonlinear dissipative effects of ferroelectric polycrystals based on firm thermodynamic principles. The developed micromechanically motivated model is embedded into an electromechanically coupled finite element formulation in which each grain is represented by a single finite element. Initial dipole directions are assumed to be randomly oriented to mimic the virgin state of the unpoled ferroelectric polycrystal. An energy-based criterion using Gibbs free energy is adopted for the initiation of the domain switching process. The key aspect of the proposed model is the incorporation of effects of the constraint imposed by the surrounding grains on a switching grain. This is accomplished by the inclusion of an additional term in the domain switching criterion that is related to the gradient of the driving forces at the boundary of the grains. To study the overall bulk ceramics behavior, a simple volume-averaging technique is adopted. It turns out that the simulations based on the developed finite element formulation with grain boundary effects are consistent with the experimental data reported in the literature.

1. Introduction

An active or ‘smart’ material is often defined as one that responds sharply to an input stimulus. The response can be in many different forms such as an electrical or magnetic response to a mechanical or a thermal input stimulus. Active materials have begun to play an important role in modern structural and intelligent systems design. Ferroelectric materials represent a popular class of active materials used in applications such as transducers, actuators and sensors. The unique electromechanical coupling in the constitutive behavior of these materials serves as a key aspect in applying these materials to smart systems. Currently, ferroelectric ceramics are widely used in various applications such as MEMS devices, FRAM (ferroelectric random access memories), nanopositioning, active damping and ultrasonics (see [33]). While these materials show a nearly linear response under the action of low electromechanical loadings, they exhibit strong nonlinear response under high loading conditions. Domain switching effects are accepted to be the main source for this

highly nonlinear behavior, stemming from the reorientation of the underlying polarization directions (see the review article by [21]). This reorientation additionally causes a change in strain termed as spontaneous strain. Therefore, it is of cardinal importance to account for this characteristic constitutive behavior in sound modeling principles; refer to [26, 15].

Ferroelectric constitutive models can be, in general, classified as macroscopic (phenomenological) models or microscopic (subgrain) models. Phenomenological models are generally derived within the thermodynamic framework. The state of the material is defined by a set of internal variables at any given time and the evolution of these internal variables are defined by means of kinetic equations [19, 24, 20, 32, 30]. Remanent strain and remanent polarization are the primary internal variables that define the irreversible state of the material. The models proposed subsequently use a plasticity approach in which the electric and the stress switching (yield) surfaces are developed and the macroscopic reversible behavior is assumed to occur within these surfaces. During the switching process, the switching surface undergoes an

irreversible change due to the change in the remanent strain and the remanent polarization. The switching surface expands or moves depending upon the hardening rule proposed that determines the evolution of the new surface [8, 31, 23, 34]. The phenomenological models are computationally effective and their implementation is quite straightforward. However, these models require a lot of constants that need to be obtained from experimental results.

The second approach that focuses on micromechanical models is based on the internal microstructure and the microscopic switching mechanisms. These models are set up with different choices of material behavior and the substructures to be incorporated into the model depending on the length scales at which the mechanisms occur. Since the origin of these models include better physical insight into the material behavior, these models are believed to be more appropriate than the phenomenological models; refer to [16, 5, 14, 2]. In general, the assumption starts with each grain consisting of a single domain or multiple domains. It is considered in the modeling and is allowed to switch when the internal electromechanical fields in the ferroelectric grain meet some switching criterion. The criterion may be based on the work done, the total potential, the Gibbs energy or the internal energy density [6, 12, 28]. The driving force for each increment of external loads is calculated and checked for the switching criterion and, upon satisfying the criterion, the existing domains are converted to another set of domains that are favorable to the external forcing fields. The macroscopic material behavior is obtained by microscopic averaging of the individual grains or domains. The high computational costs in the simulations using these models compared to the phenomenological models are offset by the minimal requirements of material constants that have to be obtained by conducting experiments.

For the numerical simulation of piezoelectric materials, the finite element method is one among the tools that can be used effectively. Allik [1] developed the finite element formulation for the underlying set of linear piezoelectric equations based on variational principles. Subsequently, nonlinear FE settings were formulated by Gaudenzi and Bathe [10] for the electromechanical coupled behavior of piezoelectric continua. Several publications are available in the literature about FEM usage for the simulation of nonlinear behavior of ferroelectrics [9, 17, 25, 22, 3, 18, 29].

The present paper deals with a thermodynamically consistent micromechanical model using a domain switching criterion that includes grain boundary effects. The main features of the present work are:

- A thermodynamically motivated, dissipation maximization-based formulation that considers domain switching processes under electromechanical coupled loading is developed.
- Boundary effects between the grains are captured via a microscopic approach by incorporating an additional term based on the change in the Gibbs free energy of the domains in the neighborhood of the switching domain. This is used as the threshold for the onset of domain switching.

- In the modeling of perovskite crystallites with tetragonal microstructure, the material parameters are related to the unit-cell orientations, i.e. material constants will change upon domain switching.
- The developed framework is embedded into a coupled finite element formulation, whereby a straightforward staggered iteration scheme is applied to solve the nonlinear coupled problem within each and every loading/time step. Initially the domains occupying individual finite elements are assumed to have random polarization directions.
- The formulation is used to simulate the response for the ferroelectric, the ferroelastic, the superimposed prestress loading and the multiaxial loading cases.

The outline of this paper is as follows: fundamental relations such as balance laws and kinetics are summarized in section 2. The thermodynamical formulation is discussed in section 3 based on state variables and thermodynamic potential. The adopted energy-based switching criterion is discussed in section 4 together with the underlying basics of boundary effects by means of a micromechanical approach. Aspects of the related implementation and algorithmic treatment embedded into an iterative finite element context and the numerical examples are included in sections 5 and 6. Finally, the paper is concluded with a short summary in section 7.

2. Fundamental equations

The configuration of a ferroelectric body Γ of interest is denoted by $\Gamma \subset \mathbb{R}^3$ and positions of material points are characterized by means of $\mathbf{x} \in \mathbb{R}^3$. The governing mechanical and electrostatic equilibrium conditions for the bulk material represent in local formats of the balance of linear momentum (in the absence of acceleration) and Gauss's law result in

$$\mathbf{0} = \nabla \cdot \boldsymbol{\sigma} + \mathbf{b} \quad \text{in } \mathcal{B} \quad \text{and} \quad \mathbf{0} = \nabla \cdot \mathbf{D} - q \quad \text{in } \mathcal{B} \quad (1)$$

where \mathbf{b} and q are the mechanical body force components and the electric charge density, respectively. $\boldsymbol{\sigma}$ and \mathbf{D} denote respectively the Cauchy stress tensor and the electric displacement. As essential degrees of freedoms we introduce the displacement field $\mathbf{u} \in \mathbb{R}^3$ and the electric potential $\phi \in \mathbb{R}$, so that the boundary conditions for the mechanical problem either prescribing the displacement \mathbf{u} on the boundary $\partial\mathcal{B}_u$ or tractions $\boldsymbol{\sigma} \cdot \mathbf{n}_\sigma$ on the boundary $\partial\mathcal{B}_\sigma$ such as

$$\mathbf{u} = \mathbf{u}^p \quad \text{on } \partial\mathcal{B}_u \quad \text{or} \quad \mathbf{t} = \mathbf{t}^p = \boldsymbol{\sigma} \cdot \mathbf{n}_\sigma \quad \text{on } \partial\mathcal{B}_\sigma. \quad (2)$$

In addition, it is subjected to electric boundary conditions with prescribed electric potential ϕ or the surface charge density $\mathbf{D} \cdot \mathbf{n}_D$ on the boundary. $\partial\mathcal{B}_\phi$ or $\partial\mathcal{B}_D$, respectively, are

$$\phi = \phi^p \quad \text{on } \partial\mathcal{B}_\phi \quad \text{or} \quad q = q^p = -\mathbf{D} \cdot \mathbf{n}_D \quad \text{on } \partial\mathcal{B}_D \quad (3)$$

with $\partial\mathcal{B}_u \cup \partial\mathcal{B}_\sigma = \partial\mathcal{B}_\phi \cup \partial\mathcal{B}_D = \partial\mathcal{B}$ as well as $\partial\mathcal{B}_u \cap \partial\mathcal{B}_\sigma = \partial\mathcal{B}_\phi \cap \partial\mathcal{B}_D = \emptyset$, and $\mathbf{n}_{\sigma,D}$ are outward unit vectors defined with respect to the surfaces $\partial\mathcal{B}_\sigma$, $\partial\mathcal{B}_D$. The kinematic relations

(between strain tensor and displacements, and between electric field and potential) in the bulk ceramic are given by

$$\boldsymbol{\varepsilon} = \frac{1}{2}(\nabla \otimes \mathbf{u} + \mathbf{u} \otimes \nabla) \text{ together with } \quad (4)$$

$$\mathbf{E} = -\nabla \phi.$$

The classical linear ansatz for the modeling of piezoelectric materials in the piezoelectric phase is

$$\mathbf{D} = \mathbf{d} : \boldsymbol{\varepsilon} + \mathbf{k} \cdot \mathbf{E} \quad \text{and} \quad \boldsymbol{\sigma} = \mathbf{C} : \boldsymbol{\varepsilon} - \mathbf{d}^T \cdot \mathbf{E} \quad (5)$$

wherein the elastic stiffness $\mathbf{C} = \mathbf{C}^t = \mathbf{C}^T \in \mathbb{R}^{3 \times 3 \times 3 \times 3}$, the dielectric permittivity $\mathbf{k} = \mathbf{k}^t \in \mathbb{R}^{3 \times 3}$ and the piezoelectric tensor $\mathbf{d} \in \mathbb{R}^{3 \times 3 \times 3}$.

3. Thermodynamical formulation

Ferroelectric materials exhibit electrical, mechanical and thermal coupled phenomena, which can be described based on a thermodynamical approach to model the material behavior.

3.1. State variables

The state variables can be split into two parts such as the observable variables and the internal variables. The electric field \mathbf{E} , the total strain $\boldsymbol{\varepsilon}$ and the temperature θ are namely the observable variables. The current state for the ferroelectrics depends on the history, which could be represented as the internal variables and subsequently these variables are associated with the dissipation phenomena. When the ferroelectric materials are subjected to higher electromechanical loading and unloading, they exhibit some electrical displacement and the total strain at zero electric field and/or at zero mechanical stress are denoted as remanent electric displacement (polarization) and remanent strain. Due to these unrecoverable values, both the electric displacement and total strain can be assumed to be decomposable into a reversible part with a $\{\bullet^r\}$ and an irreversible part with $\{\bullet^i\}$ as (see also [4])

$$\mathbf{D} = \mathbf{D}^r + \mathbf{D}^i \quad \text{and} \quad \boldsymbol{\varepsilon} = \boldsymbol{\varepsilon}^r + \boldsymbol{\varepsilon}^i. \quad (6)$$

At the microscopic level, the unit cell of the considered ferroelectric material possesses cubic symmetry for operating temperatures above the Curie temperature. This phase is called paraelectric whereby the relative atom positions in the crystal lattice give rise to a vanishing net dipole moment which gives no piezoelectric effect. However, below the Curie temperature, the symmetry of the material might switch from simple cubic structures to tetragonal or rhombohedral arrangements. The new phase is denoted as the ferroelectric phase, in which relative atom positions in the crystal lattice might change which gives rise to nonzero net dipole moments that are usually introduced as spontaneous polarization (vectors). During such phase transitions, the movements of atoms apparently result in lattice distortions which consequently cause mechanical strain, termed as spontaneous strain. For polycrystalline materials in the virgin or unpoled state, the polarization vector field is in general randomly oriented. Practically speaking, each grain

is divided into domains of different polarization orientations. Since the direction of polarization is equally distributed in the virgin state, the net polarization and the strain of the bulk material vanish at the macrolevel. If the material is subjected to external loads either electrical (a prescribed electric field) and/or mechanical traction, the lattice structure undergoes a recoverable change in polarization and strain with the existing domain type. When the loads exceed a certain limit, the unit cell may reorient in a way that the polarization vectors within the grains align according to this loading direction. This change in domain type in ferroelectrics is referred to as domain switching and is irreversible in nature. As the external loads increase, a specific domain type is favored at the expense of others. Domain switching may initiate at the boundaries, in general on the surface, and propagates inside, and/or it may nucleate at various regions in the material and move towards each other.

In a ferroelectric crystal structure, the remanent quantities represent macroscopic averages of the microscopic spontaneous polarization and strain. Based on this argument, in this micromechanical model the remanent polarization and strain are assumed to be equivalent to the spontaneous polarization \mathbf{P}^s and strain $\boldsymbol{\varepsilon}^s$. The nonlinear constitutive equations of the ferroelectric material additionally incorporate a spontaneous polarization vector and a spontaneous strain tensor. The extension of equation (5) consequently renders

$$\mathbf{D} = \mathbf{d} : [\boldsymbol{\varepsilon} - \boldsymbol{\varepsilon}^s] + \mathbf{k} \cdot \mathbf{E} + \mathbf{P}^s \quad \text{and} \quad (7)$$

$$\boldsymbol{\sigma} = \mathbf{C} : [\boldsymbol{\varepsilon} - \boldsymbol{\varepsilon}^s] - \mathbf{d}^T \cdot \mathbf{E}.$$

Experimental investigations reported that, during domain switching, almost all the material constants of a ferroelectric polycrystalline will change. Since we are particularly interested in the modeling of perovskite crystallites with tetragonal microstructure, the material parameters are incorporated in relation with unit-cell orientations. The elastic tensor, however, which will be enabled to vary from domain to domain, allows the representation

$$\mathbf{C} := \lambda \mathbf{I} \otimes \mathbf{I} + 2\mu_T \mathbf{I}^{\text{sym}} + \alpha [\mathbf{I} \otimes \mathbf{M} + \mathbf{M} \otimes \mathbf{I}] + 2\mu_E [\mathbf{I} \underline{\otimes} \mathbf{M} + \mathbf{M} \underline{\otimes} \mathbf{I}] + \beta \mathbf{M} \quad (8)$$

with \mathbf{m} as the unit-cell orientation, $\mathbf{M} := \mathbf{m} \otimes \mathbf{m}$, $\mathbf{M} := \mathbf{M} \otimes \mathbf{M}$, $\mu_E := [\mu_L - \mu_T]$ and $\mathbf{I}^{\text{sym}} := \frac{1}{2}[\mathbf{I} \underline{\otimes} \mathbf{I} + \mathbf{I} \underline{\otimes} \mathbf{I}]$. The non-standard dyadic products $(\mathbf{A} \underline{\otimes} \mathbf{B})_{ijkl} = A_{il} B_{jk}$, $(\mathbf{A} \overline{\otimes} \mathbf{B})_{ijkl} = A_{ik} B_{jl}$. In view of the piezoelectric tensor, one similarly ends up with

$$\mathbf{d} := -d_{31} \mathbf{m} \otimes \mathbf{I} - d_{33} \bar{\mathbf{M}} - \frac{1}{2} d_{15} [\mathbf{I} \otimes \mathbf{m} + \mathbf{I} \overline{\otimes} \mathbf{m}], \quad (9)$$

$$\mathbf{d}^T := -d_{31} \mathbf{I} \otimes \mathbf{m} - d_{33} \bar{\mathbf{M}} - \frac{1}{2} d_{15} [\mathbf{I} \overline{\otimes} \mathbf{m} + \mathbf{m} \otimes \mathbf{I}]$$

wherein $\bar{\mathbf{M}} := \mathbf{m} \otimes \mathbf{M}$ and the dielectric permittivity is

$$\mathbf{k} := -2k_{11} \mathbf{I} - 2k_{33} \mathbf{M}. \quad (10)$$

3.2. Thermodynamic potential and evolution laws

The dissipation can be derived based on the existence of a thermodynamic potential as

$$\rho(\theta \dot{s} - \dot{u}) + \boldsymbol{\sigma} : \dot{\boldsymbol{\varepsilon}}^r + \mathbf{E} \cdot \dot{\mathbf{D}}^r + \boldsymbol{\sigma} : \dot{\boldsymbol{\varepsilon}}^i + \mathbf{E} \cdot \dot{\mathbf{D}}^i - \frac{1}{\theta} \mathbf{q} \cdot \text{Grad } \theta \geq 0 \quad (11)$$

with ρ as the density, θ the temperature, s the specific entropy, u the specific internal energy and \mathbf{q} the heat flux vector.

The Gibbs free energy for a single crystal can be expressed as the function of observable state variables \mathbf{E} , $\boldsymbol{\sigma}$, θ and internal variable ζ^α as

$$G = G(\boldsymbol{\sigma}, \mathbf{E}, \theta, \zeta^\alpha) \quad (12)$$

where ζ^α is the internal variable for the particular domain type α among the six distinct domain structures. Here we neglected the volume fraction within a single crystal and the interface contributions between the domains:

$$\dot{G} = \frac{\partial G}{\partial \boldsymbol{\sigma}} \dot{\boldsymbol{\sigma}} + \frac{\partial G}{\partial \mathbf{E}} \dot{\mathbf{E}} + \frac{\partial G}{\partial \theta} \dot{\theta} + \frac{\partial G}{\partial \zeta^\alpha} \dot{\zeta}^\alpha. \quad (13)$$

The resulting dissipation inequality can be derived by using Legendre transformation and equation (13) as

$$\begin{aligned} & - \left[\rho \frac{\partial G}{\partial \boldsymbol{\sigma}} + \boldsymbol{\varepsilon}^r \right] \cdot \dot{\boldsymbol{\sigma}} - \left[\rho \frac{\partial G}{\partial \mathbf{E}} + \mathbf{D}^r \right] \cdot \dot{\mathbf{E}} \\ & - \left[\rho \frac{\partial G}{\partial \theta} + \rho \eta \right] \cdot \dot{\theta} - \rho \frac{\partial G}{\partial \zeta^\alpha} \cdot \dot{\zeta}^\alpha \\ & + \boldsymbol{\sigma} : \dot{\boldsymbol{\varepsilon}}^i + \mathbf{E} \cdot \dot{\mathbf{D}}^i - \frac{1}{\theta} \mathbf{q} \cdot \text{Grad } \theta \geq 0. \end{aligned} \quad (14)$$

Equation (14) holds for $\boldsymbol{\sigma}$, \mathbf{E} and θ are controllable variables and will vanish under mechanical, electrical and thermal equilibrium conditions. Assuming isothermal processes and homogeneous temperature fields, equation (14) can be simplified as

$$\boldsymbol{\sigma} : \dot{\boldsymbol{\varepsilon}}^i + \mathbf{E} \cdot \dot{\mathbf{D}}^i - \rho \frac{\partial G}{\partial \zeta^\alpha} \cdot \dot{\zeta}^\alpha \geq 0. \quad (15)$$

The irreversible strain ($\boldsymbol{\varepsilon}^i$) and polarization (\mathbf{D}^i) can be expressed as a function of ζ^α as

$$\boldsymbol{\varepsilon}^i = \boldsymbol{\varepsilon}^i(\zeta^\alpha) = \boldsymbol{\varepsilon}^* \cdot \zeta^\alpha \quad \text{and} \quad \mathbf{D}^i = \mathbf{D}^i(\zeta^\alpha) = \mathbf{D}^* \cdot \zeta^\alpha \quad (16)$$

where $\boldsymbol{\varepsilon}^*$ and \mathbf{D}^* are transformation strain and electrical displacement, respectively. Using this assumption, the generalized dissipation inequality for the ferroelectrics can be expressed as

$$\begin{aligned} & \boldsymbol{\sigma} : \boldsymbol{\varepsilon}^* \dot{\zeta}^\alpha + \mathbf{E} \cdot \mathbf{D}^* \dot{\zeta}^\alpha - \rho \frac{\partial G}{\partial \zeta^\alpha} \cdot \dot{\zeta}^\alpha \geq 0 \\ & \Rightarrow \left[\boldsymbol{\sigma} : \boldsymbol{\varepsilon}^* + \mathbf{E} \cdot \mathbf{D}^* - \rho \frac{\partial G}{\partial \zeta^\alpha} \right] \cdot \dot{\zeta}^\alpha \geq 0. \end{aligned} \quad (17)$$

4. Switching criterion

4.1. Driving force and critical energy

In this section, the generalized thermodynamic aspects are narrowed towards the microscopic level of ferroelectrics. The dissipation potential in equation (17) gives the product of thermodynamic driving force for transformation ($\boldsymbol{\sigma} : \boldsymbol{\varepsilon}^* + \mathbf{E} \cdot \mathbf{D}^* - \rho \frac{\partial G}{\partial \zeta^\alpha}$) and the rate at which the volume fraction (ζ^α) of a particular domain type evolves. An application of external loads, on reaching a critical level, the underlying unit cell or domain switches from one state to the other possible states;

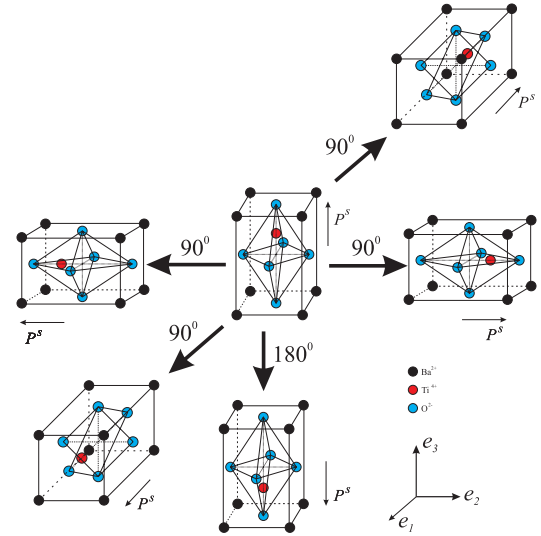


Figure 1. 90° and 180° domain switching types for a representative tetragonal lattice structure.

(This figure is in colour only in the electronic version)

refer to figure 1. The phase transformation refers to a switching process in which the change in spontaneous polarization and strain occurs; assume the present domain type β switches to the other domain type α in the unit cell. The transformation strain and displacement or polarization yields

$$\begin{aligned} \boldsymbol{\varepsilon}^* &= \Delta \boldsymbol{\varepsilon}_{\beta \rightarrow \alpha}^s = \boldsymbol{\varepsilon}_\alpha^s - \boldsymbol{\varepsilon}_\beta^s \quad \text{and} \\ \mathbf{D}^* &= \Delta \mathbf{P}_{\beta \rightarrow \alpha}^s = \mathbf{P}_\alpha^s - \mathbf{P}_\beta^s. \end{aligned} \quad (18)$$

The reversible bulk Gibbs energy of this crystal G can be expressed as (assume only two domain types α and β)

$$G = \zeta^\alpha G^\alpha + \zeta^\beta G^\beta = G^\beta + \Delta G^{\alpha-\beta} \zeta^\alpha \quad (19)$$

where

$$\begin{aligned} \Delta G^{\alpha-\beta} &= G^\alpha - G^\beta = - \left[\frac{1}{2} \boldsymbol{\sigma} : (\mathbf{C}_\alpha - \mathbf{C}_\beta) : \boldsymbol{\sigma} \right. \\ & \left. + \frac{1}{2} \mathbf{E} \cdot (\mathbf{k}_\alpha - \mathbf{k}_\beta) \cdot \mathbf{E} + \mathbf{E} \cdot (\mathbf{d}_\alpha - \mathbf{d}_\beta) : \boldsymbol{\sigma} \right]. \end{aligned} \quad (20)$$

Here, ζ^α and ζ^β refer to the volume fractions of domains α and β , respectively, and the constraint is $\zeta^\alpha + \zeta^\beta = 1$. Inserting equation (18) and the derivative of equation (19) in equation (17) yields the dissipation potential for the phase transformation or domain switching occurring from β to α type in a unit cell of ferroelectrics which can be expressed as

$$\begin{aligned} & (\boldsymbol{\sigma} : \Delta \boldsymbol{\varepsilon}_{\beta \rightarrow \alpha}^s + \mathbf{E} \cdot \Delta \mathbf{P}_{\beta \rightarrow \alpha}^s + \frac{1}{2} \boldsymbol{\sigma} : (\mathbf{C}_\alpha - \mathbf{C}_\beta) : \boldsymbol{\sigma} \\ & + \frac{1}{2} \mathbf{E} \cdot (\mathbf{k}_\alpha - \mathbf{k}_\beta) \cdot \mathbf{E} \\ & + \mathbf{E} \cdot (\mathbf{d}_\alpha - \mathbf{d}_\beta) : \boldsymbol{\sigma}) \cdot \dot{\zeta}^\alpha \geq 0 \Rightarrow f^{\text{drv}} \cdot \dot{\zeta}^\alpha \geq 0. \end{aligned} \quad (21)$$

For the domain switching, the energy is dissipated by domain wall motion upon transforming a unit volume of crystal from one state to the next state by operation of the transformation system. The thermodynamic driving force (f^{drv}) must satisfy the following inequality at all times. Then there is a possibility of phase transformation:

$$f^{\text{drv}} \dot{\zeta}^\alpha \leq f^{\text{crit}} \dot{\zeta}^\alpha. \quad (22)$$

For the phase transformations within the $\langle 100 \rangle$ family, six different states or orientations of the particular unit cell of interest come into the picture—the initial state, four types of 90° domain switching and 180° domain switching. For the pure mechanical (spontaneous strain) state, four 90° strain switching states have to be considered. On the other hand, for the electrical (spontaneous polarization) state four 90° switching states together with one 180° switching state have to be considered. From the experimental results, it is observed that the switching thresholds are varying throughout the loading [35]. The present work incorporates the critical energy barrier in which the underlying mechanism for 90° switchings and 180° switchings are different, which gives the critical values for their occurrence are also different. Assuming the electrical loading contributes for direct 180° switching and apply the condition in equations (21) and (22), which gives the critical value for 180° switching as follows:

$$\begin{aligned} f_{180}^{\text{crit}} &= \mathbf{E} \cdot \Delta \mathbf{P}_{\beta \rightarrow \alpha}^s + \frac{1}{2} \mathbf{E} \cdot (\mathbf{k}_\alpha - \mathbf{k}_\beta) \cdot \mathbf{E} \\ &= 2E_c P_0 + 0 = 2E_c P_0 \end{aligned} \quad (23)$$

where E_c is the coercive electric field; the change in spontaneous polarization $\Delta \mathbf{P}_{\beta \rightarrow \alpha}^s = 2\mathbf{P}^s = 2P_0$; P_0 is the spontaneous polarization; the dielectric constant $(\mathbf{k}_\alpha - \mathbf{k}_\beta)$ between two states is unchanged for 180° switching. The critical value for 90° switching gives

$$\begin{aligned} f_{90}^{\text{crit}} &= \mathbf{E} \cdot \Delta \mathbf{P}_{\beta \rightarrow \alpha}^s + \frac{1}{2} \mathbf{E} \cdot (\mathbf{k}_\alpha - \mathbf{k}_\beta) \cdot \mathbf{E} \\ &= E_c P_0 + \frac{1}{2} E_c^2 \cdot (\mathbf{k}_{33} - \mathbf{k}_{11}). \end{aligned} \quad (24)$$

Regarding the ferroelastic switching case, it exhibits only 90° switching due to the application of pure mechanical stress which yields

$$\begin{aligned} f_{90\text{ela}}^{\text{crit}} &= \boldsymbol{\sigma} : \Delta \boldsymbol{\varepsilon}_{\beta \rightarrow \alpha}^s + \frac{1}{2} \boldsymbol{\sigma} : (\mathbf{C}_\alpha - \mathbf{C}_\beta) : \boldsymbol{\sigma} \\ &= \frac{3}{2} \sigma_c \varepsilon_0 + \frac{1}{2} \sigma_c^2 \cdot (C_{3333} - C_{1111}) \end{aligned} \quad (25)$$

where σ_c is the coercive stress; $\boldsymbol{\varepsilon}^s = \varepsilon_0$ is the spontaneous strain, and C_{3333} and C_{1111} are the compliance constants.

4.2. Grain boundary effects

Polycrystalline microstructures often give rise to local loading levels that could be significantly different from the loading levels expected from the boundary conditions applied to the entire specimen. Moreover, individual grains and domains, possibly possessing different polarization directions, interact with the neighboring grains which are often described as grain boundary effects or intergranular effects. Domain switching might occur at macroscopic loading levels that are different from the established coercive values of single grains, thus introducing nonlinear effects even within small loading ranges. In this model, we consider one crystal per element and the interactions among the domains are taken into account and integrated into an electromechanically coupled finite element formulation.

When no domain switching occurs, the spatial variation of the Gibbs free energy is expected to be generally smooth. When the domain switching occurs, there is an abrupt change of Gibbs free energy in the switching domain that may disturb the smoothness of the spatial variation of the Gibbs free energy.

In other words, a sharp jump in the Gibbs free energy at the boundaries of the switching domain occurs in the numerical setting. To avoid such a non-physical sharp change in the Gibbs free energy in the computations, a boundary effect needs to be included to introduce smoothness into the Gibbs energy function variation. The smoothing can be effected in much the same way as in stress smoothing procedures. In this work smoothing of the Gibbs free energy is done using a simple method proposed in [7]. In smoothing, the free energy levels get altered and this can be considered to be due to the interactions between the grains. An approximate numerical gradient is computed using the difference in the neighboring domain driving forces and the driving force at the switching domain. This gradient is assumed, in this model to play a role in the domain switching criterion, thus introducing the gradient effects in the model indirectly as

$$\begin{aligned} f_0^{\text{drv}} + \{\text{gradient at the boundary of the switching domain}\} \\ \geq f^{\text{crit}}. \end{aligned} \quad (26)$$

The gradient of the driving force with a neighboring domain can be approximated by the normalized difference between the neighboring domain driving forces (f_i^{drv}) and the driving force at the switching domain (f_0^{drv}) as

$$f_0^{\text{drv}} + \frac{f_i^{\text{drv}} - f_0^{\text{drv}}}{d} \geq f^{\text{crit}} \quad (27)$$

where d is the normalizing-scale-dependent quantity and i represents the several neighborhood domains. The above expression can be rewritten as

$$(f_0^{\text{drv}})_{\text{effective}} = (1 - \bar{p}) f_0^{\text{drv}} + \bar{p} f_i^{\text{drv}} \quad (28)$$

where \bar{p} absorbs the effect of the quantity d .

The scale-dependent material parameter d (and thus p) could be different for different energies—electrical, mechanical and electromechanical. Therefore, we generalize the formulation by introducing different parameters for the different energies and an additional term based on the gradient with the other domains is used as the threshold for the onset of domain switching. Thus

$$\begin{aligned} \left[(f_0^{\text{drv}})_{\text{effective}} = \left(1 - \frac{p}{2}\right) f_0^{\text{drv}} + \left(\frac{p_{i-e}}{2}\right) f_{i-e}^{\text{drv}} \right. \\ \left. + \left(\frac{p_{i-m}}{2}\right) f_{i-m}^{\text{drv}} + \left(\frac{p_{i-em}}{2}\right) f_{i-em}^{\text{drv}} \right] \geq f^{\text{crit}} \end{aligned} \quad (29)$$

where f_0^{drv} is the driving force of the switching domain while f_{i-e}^{drv} , f_{i-m}^{drv} , f_{i-em}^{drv} are the electrical, mechanical and electromechanical driving forces of the neighboring or surrounding domains of the switching domain. $p = \frac{p_{i-e}^{\text{drv}} + p_{i-m}^{\text{drv}} + p_{i-em}^{\text{drv}}}{3}$, $0 < p \leq 1$ and p_{i-e}^{drv} , p_{i-m}^{drv} , p_{i-em}^{drv} are the

corresponding material-dependent parameters:

$$\begin{aligned}
 f_0^{\text{drv}} &= \boldsymbol{\sigma} : \Delta \boldsymbol{\varepsilon}_{\beta \rightarrow \alpha}^s + \mathbf{E} \cdot \Delta \mathbf{P}_{\beta \rightarrow \alpha}^s + \Delta G_{\alpha-\beta} \\
 f_{i-e}^{\text{drv}} &= \frac{1}{n} \sum_{i=1}^n \left[\mathbf{E}^{(i)} \cdot \Delta \mathbf{P}_{\beta \rightarrow \alpha}^{s(i)} + \frac{1}{2} \mathbf{E}^{(i)} \cdot (\mathbf{k}_\alpha - \mathbf{k}_\beta)^{(i)} \cdot \mathbf{E}^{(i)} \right] \\
 f_{i-m}^{\text{drv}} &= \frac{1}{n} \sum_{i=1}^n \left[\boldsymbol{\sigma}^{(i)} : \Delta \boldsymbol{\varepsilon}_{\beta \rightarrow \alpha}^{s(i)} + \frac{1}{2} \boldsymbol{\sigma}^{(i)} : (\mathbf{C}_\alpha - \mathbf{C}_\beta)^{(i)} : \boldsymbol{\sigma}^{(i)} \right] \\
 f_{i-em}^{\text{drv}} &= \frac{1}{n} \sum_{i=1}^n [\mathbf{E}^{(i)} \cdot (\mathbf{d}_\alpha - \mathbf{d}_\beta)^{(i)} : \boldsymbol{\sigma}^{(i)}]
 \end{aligned} \quad (30)$$

where $\Delta G_{\alpha-\beta} = \frac{1}{2} \boldsymbol{\sigma} : (\mathbf{C}_\alpha - \mathbf{C}_\beta) : \boldsymbol{\sigma} + \frac{1}{2} \mathbf{E} \cdot (\mathbf{k}_\alpha - \mathbf{k}_\beta) \cdot \mathbf{E} + \mathbf{E} \cdot (\mathbf{d}_\alpha - \mathbf{d}_\beta) : \boldsymbol{\sigma}$; $\{\bullet\}^{(i)}$ indicates the electric field, stress and material constants for the surrounding domains; n is the number of surrounding domains. In this model, n is considered as eight surrounding domains in general. However it will vary in some specific cases; for instance, if the switching domains are at the corner of the specimen, then n will be three surrounding domains; if the switching domains are at the edges, the number of surrounding domains, n might be five. Substituting equation (30) in equation (29) yields

$$\begin{aligned}
 (f_0^{\text{drv}})_{\text{effective}} &= \left(1 - \frac{p_{i-e} + p_{i-m} + p_{i-em}}{6} \right) f_0^{\text{drv}} \\
 &+ \left(\frac{p_{i-e}}{2} \right) \frac{1}{n} \sum_{i=1}^n [\mathbf{E}^{(i)} \cdot \Delta \mathbf{P}_{\beta \rightarrow \alpha}^{s(i)} \\
 &+ \frac{1}{2} \mathbf{E}^{(i)} \cdot (\mathbf{k}_\alpha - \mathbf{k}_\beta)^{(i)} \cdot \mathbf{E}^{(i)}] \\
 &+ \left(\frac{p_{i-m}}{2} \right) \frac{1}{n} \sum_{i=1}^n [\boldsymbol{\sigma}^{(i)} : \Delta \boldsymbol{\varepsilon}_{\beta \rightarrow \alpha}^{s(i)} \\
 &+ \frac{1}{2} \boldsymbol{\sigma}^{(i)} : (\mathbf{C}_\alpha - \mathbf{C}_\beta)^{(i)} : \boldsymbol{\sigma}^{(i)}] \\
 &+ \left(\frac{p_{i-em}}{2} \right) \frac{1}{n} \sum_{i=1}^n [\mathbf{E}^{(i)} \cdot (\mathbf{d}_\alpha - \mathbf{d}_\beta)^{(i)} : \boldsymbol{\sigma}^{(i)}] \geq f^{\text{crit}}. \quad (31)
 \end{aligned}$$

5. Algorithmic setting

The subsequent numerical examples are based on a three-dimensional finite element framework wherein the above elaborated switching model is embedded. Both spontaneous polarization \mathbf{P}^s as well as spontaneous strains $\boldsymbol{\varepsilon}^s$ are thereby introduced as internal variables stored at the integration point level or, for the problem at hand, at the element level. Here, we will not distinguish between grains and domains but rather attach an individual grain orientation, as represented by $\{\mathbf{m}_{1,2,3}\}$ by a single (eight-node brick) finite element. For the computation aspects, the initial unit-cell orientation (\mathbf{m}), which also determines the initial polarization vector ($\mathbf{P}^s = P^s \mathbf{m}$) and the initial spontaneous strains ($\boldsymbol{\varepsilon}^s = \varepsilon^s [3\mathbf{M} - \mathbf{I}]/2$), for $\varepsilon^s > 0$ are considered. Random orientations ($\mathbf{M} = \mathbf{m} \otimes \mathbf{m}$) are applied by using Eulerian angles ($\Phi, \Psi \in [0, 2\pi)$, $\sin(\Theta - \frac{\pi}{2}) \in [-1, 1]$); see the monograph by Goldstein [11] for detailed background information. In this numerical set-up, the applied switching criterion will be referred to quantities averaged over single finite elements, namely

$$f_e^{\text{drv}}(\langle \boldsymbol{\sigma}_n \rangle_e, \langle \mathbf{E}_n \rangle_e, \mathbf{m}_n, \mathbf{m}_{n+1}) \leq f^{\text{crit}} \quad (32)$$

wherein $\langle \bullet \rangle_e = [\mathcal{V}_e]^{-1} \int_{\mathcal{V}_e} \bullet dv$ for \mathcal{V}_e denoting the volume of a particular finite element \mathcal{B}_e . To compare the simulated results with experimental data and for the purpose of visualization, projections with respect to the macroscopic loading direction \mathbf{e} are performed, namely

$$\begin{aligned}
 \mathbf{S} &= \langle \mathbf{e} \cdot \boldsymbol{\sigma} \cdot \mathbf{e} \rangle, & \mathbf{e} &= \langle \mathbf{e} \cdot \boldsymbol{\varepsilon} \cdot \mathbf{e} \rangle, \\
 \mathbf{D} &= \langle \mathbf{D} \cdot \mathbf{e} \rangle, & \mathbf{E} &= \langle \mathbf{E} \cdot \mathbf{e} \rangle
 \end{aligned} \quad (33)$$

with the global volume-averaging $\langle \bullet \rangle = [\mathcal{V}]^{-1} \int_{\mathcal{B}} \bullet dv$, where \mathcal{V} characterizes the volume of the entire body \mathcal{B} . The developed rate-independent evolution is solved by using a simple staggered iteration technique applied within each load step to incorporate switching effects as follows:

- (i) based on the coupled finite element formulation, compute \mathbf{u} and ϕ for the initial orientations.
- (ii) Fixing \mathbf{u} and ϕ , calculate the energy barrier for switching based on equations (31) and (32) for all five possibilities for each element and identify the number of elements n_{tot} that exceed the critical value based on the largest energy reduction. Since an element with a higher energy reduction is more likely to switch than an element with a lower energy reduction, the n_{tot} elements are prioritized based on their maximum local Gibbs free energy with the one possessing the highest maximum energy reduction ranked first in the list. These elements will be referred to as switching elements.
- (iii) For the first switching element, recompute \mathbf{u} and ϕ for updated grain orientations for given boundary and loading conditions.
- (iv) Steps (ii) and (iii) are repeated in the sequence of the second, the third, etc, and finally the n_{tot} switching elements to obtain a fully equilibrated state.
- (v) Finally, at the global level, the volume averaged \mathbf{S} , \mathbf{e} , \mathbf{E} and \mathbf{D} are computed based on the Reuss approximation.

For convenience of the reader, table 1 gives the algorithmic treatment of the finite element model proposed.

6. Numerical examples

All numerical examples studied in the following refer to a $10 \times 10 \times 10$ cube-shaped specimen, whereby the discretization is performed with $10 \times 10 \times 10$ eight-noded bricks (Q1Q1). In view of material parameters, representative PIC 151 values have been adopted from the literature: $k_{11} = 0.0198$ ($\mu\text{F m}^{-1}$), $k_{33} = 0.024$ ($\mu\text{F m}^{-1}$), $d_{33} = 0.45 \times 10^{-9}$ (m V^{-1}), $d_{31} = -0.21 \times 10^{-9}$ (m V^{-1}), $d_{15} = 0.58 \times 10^{-9}$ (m V^{-1}), $\lambda = 17.48$ (GPa), $\mu_L = 2.46$ (GPa), $\mu_T = 11.65$ (GPa), $\alpha = 1.67$ (GPa), $\beta = -20.74$ (GPa), $\varepsilon^s = 2.75 \times 10^{-3}$, $P^s = P_0 = 0.3$ (C m^{-2}), $E_0 = 0.7$ (MV m^{-1}), $\sigma_0 = 75$ (MPa), $p_{i-e}^{\text{drv}} = 0.7$, $p_{i-m}^{\text{drv}} = 0.5$ and $p_{i-em}^{\text{drv}} = 0.9$.

The boundary condition for the specimen under cyclic electrical loading is represented by a prescribed electric potential at the top surface ϕ_{top}^p and a zero electric potential at the bottom surface ϕ_{bot}^p . In addition compressive stress (prestress) is uniformly applied to the top surface, $\mathbf{t}_{\text{top}}^p$, and the bottom surface is clamped such that only the direction in

Table 1. Flowchart of the finite element algorithm: staggered iteration scheme.

1. random initialization of $\{\mathbf{m}_{1,2,3}\}_n$ (element level)
$\rightarrow \{\boldsymbol{\varepsilon}^s, \mathbf{P}^s, \mathbf{k}, \mathbf{C}, \mathbf{d}\}_n$
2. for global boundary conditions given (local level)
(i) $\boldsymbol{\varepsilon}_{en} = \nabla_{\mathbf{x}}^{\text{sym}} \mathbf{u}_n - \boldsymbol{\varepsilon}_n^s, \quad \mathbf{E}_n = -\nabla_{\mathbf{x}} \phi_n$
(ii) $\boldsymbol{\sigma}_n(\boldsymbol{\varepsilon}_{en}, \mathbf{E}_n, \mathbf{m}_n)$
3. switching criterion and update (element level)
(i) $\Delta\{\boldsymbol{\varepsilon}^s, \mathbf{P}^s, \mathbf{k}, \mathbf{C}, \mathbf{d}\}$ for $\mathbf{m} \in \{\pm \mathbf{m}_1, \pm \mathbf{m}_2, -\mathbf{m}_3\}_n$
(ii) $\langle \mathbf{E} \rangle_n^e, \langle \boldsymbol{\sigma} \rangle_n^e \rightarrow \max f^{drv}$
if switching criterion is not met goto 4.
else
$\mathbf{P}_{n+1}^s = \mathbf{P}_n^s + \Delta \mathbf{P}^s$
$\boldsymbol{\varepsilon}_{n+1}^s = \boldsymbol{\varepsilon}_n^s + \Delta \boldsymbol{\varepsilon}^s$
$\rightarrow \{\boldsymbol{\varepsilon}^s, \mathbf{P}^s, \mathbf{k}, \mathbf{E}, \mathbf{d}\}_{n+1}$
4. for global boundary conditions given (local level)
(i) $\boldsymbol{\varepsilon}_e = \nabla_{\mathbf{x}}^{\text{sym}} \mathbf{u}_n - \boldsymbol{\varepsilon}^s, \quad \mathbf{E} = -\nabla_{\mathbf{x}} \phi_n$
(ii) $\boldsymbol{\sigma}(\boldsymbol{\varepsilon}_e, \mathbf{E}, \mathbf{m}), \quad \mathbf{D}(\boldsymbol{\varepsilon}_e, \mathbf{E}, \mathbf{m})$
endif
5. for global boundary conditions given (global level)
(i) assembly and update \mathbf{u}, ϕ
(ii) compute $\mathbf{S}, \mathbf{e}, \mathbf{D}, \mathbf{E}$

which the traction is applied is set to be zero, i.e. one degree of freedom. Moreover, the remaining surfaces are free from traction and charge.

6.1. Cyclic electrical loading

The simulation starts with solely cyclic electrical loading without any prescribed mechanical stresses. The starting point for the first cycle is at zero potential for the macroscopically unpoled ceramic, whereby randomly oriented polarization vectors, spontaneous strains and material constants are incorporated, respectively. The electric field is applied incrementally until $+2.0$ (MV m^{-1}) and unloaded to zero field. Subsequently, the field is applied in the reverse direction to -2.0 (MV m^{-1}) and once again, the load is applied until $+2.0$ (MV m^{-1}) as a cyclic loading. Classical hysteresis and butterfly curves are showed in figure 2, i.e. the electrical displacement \mathbf{D} and total strain \mathbf{e} are monitored with respect to the electric field \mathbf{E} . The macroscopic behavior exhibits linear response starting from the origin to nearer to the coercive field 0.7 (MV m^{-1}), while the remanent strain remains zero. The electric field (0.7 (MV m^{-1})) at which switching initiates under pure electrical loading is referred to as the coercive field. Once the applied load exceeds the coercive field, then switching starts. This causes a change in spontaneous polarization and strain which obviously renders a nonlinear

macroscopic response of the electric displacement and the total strain. The applied load then reaches 2.0 (MV m^{-1}), which is referred to as the saturated level; at this stage, almost all the domains are closely aligned to the direction of the applied field. Further increase of the electric field will cause a linear response, since all the elements are already switched. When the field is unloaded, the electric displacement and strain vary linearly. At zero electric field, it exhibits some electric displacement and strain, which are called the remanent polarization and strain. Upon the application of a negative electric field, the switching processes recommence and a significant reverse poling then takes place. During the forward loading the elements are oriented in a particular direction, but in the reverse loading the oriented elements should be reoriented and aligned along the same axis but in the opposite direction, which makes the element undergo 180° switching. Concerning the strain response, during the reverse loading, the strain decreases nonlinearly to a minimum level and then starts increasing as the elements undergo reverse poling. Since the elements undergo two consecutive 90° switches to align with the negative loading direction, the strain response decreases initially for the first 90° switching and subsequently the second 90° switching occurs which makes the strain increase. The simulated results without considering the boundary effects (dotted line) show that the curves possess sharp corners near the macroscopic coercive electric field, which is not observed in experiments. However, the results with boundary effects (continuous line) show the smoothness of the curves near the critical macroscopic electric field. By comparing the simulated results (with and without boundary effects) in figure 2, the considered boundary effect plots closely match the experimental results reported by Zhou [36].

6.2. Mechanical depolarization loading

In the absence of an electric field, i.e. in the ferroelastic case, the mechanical depolarization response is predicted in terms of stress \mathbf{S} versus strain \mathbf{e} and versus dielectric displacement \mathbf{D} as shown in figure 3. The simulation is carried out considering the test specimen from the unpoled virgin state, in which the initial random orientations give rise to net zero strain and dielectric displacement. Once the incrementally applied compressive stress approaches the coercive level, say for instance -75 (MPa), then the domain switching process is initiated. Saturation is reached at a loading level of -400 (MPa) so that any further increase in the applied stresses renders an entirely linear response. Considering the ferroelastic case, the elements will undergo only four possible 90° switchings. Upon reversing the loading direction, dissipative effects as reflected by the irreversible behavior are clearly displayed. Moreover, one observes different slopes in, for example, the stress \mathbf{S} versus the strain \mathbf{e} response, which stems from aligning the local material properties according to the switching directions. From figure 3, the numerical results are found to compare reasonably well with the experimental data reported by Zhou [37].

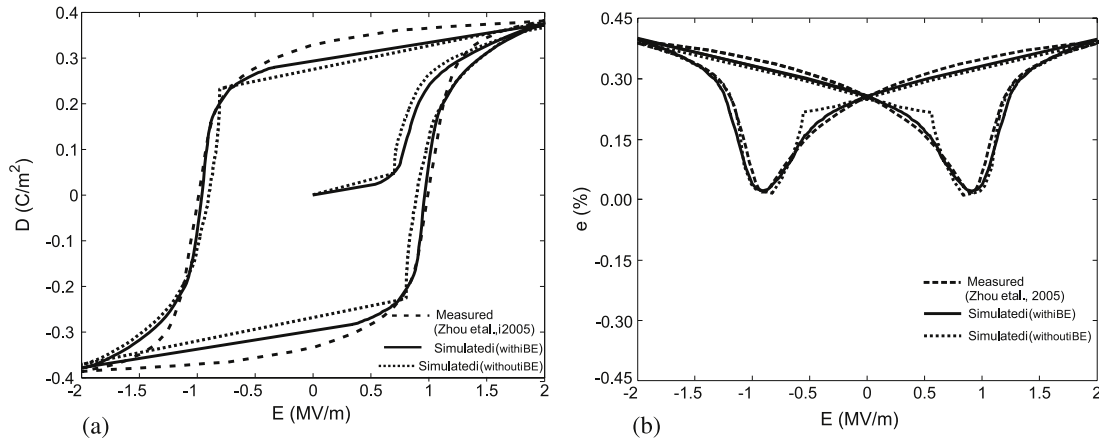


Figure 2. Hysteresis and butterfly curves—cyclic uniaxial electrical loading.

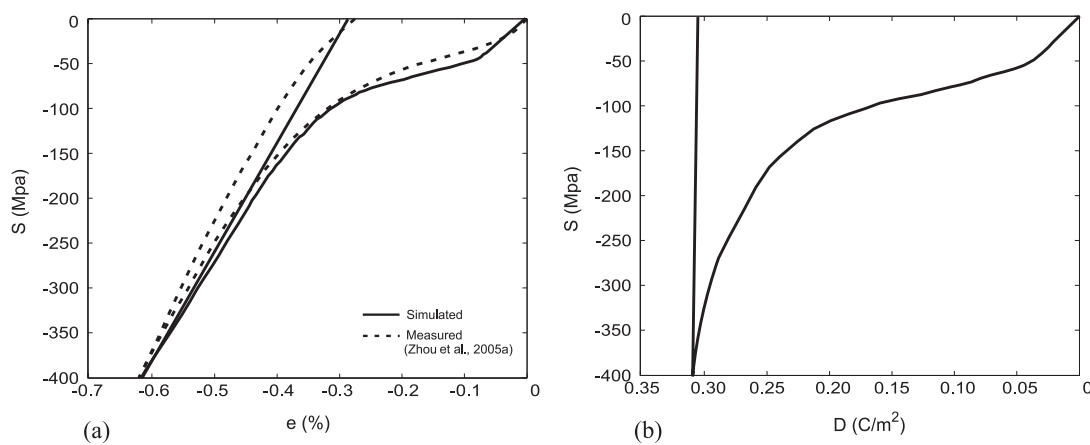


Figure 3. Stress versus strain and versus electric displacement curves—uniaxial mechanical loading.

6.3. Uniaxial ferroelectric response under constant compressive stress

Lynch [27] conducted an experiment to study the hysteresis and butterfly curves under constant compressive stress. Therein, the specimen was first poled by loading the electric field to certain values and unloaded to zero field, which results in a remanent polarization in the specimen. Then, a uniaxial compressive stress was applied on the poled specimen and the compressive stress was maintained at a certain value and a cyclic electrical loading was applied to the specimen, to capture the hysteresis and butterfly behavior under constant compressive stress. Thus, a previously poled specimen was first partially depoled by compressive stress, and cyclic electrical loading was applied to observe the response with the constant mechanical load. These experiments were repeated for different values of constant compressive stress and the ferroelectric responses were obtained. We performed the subsequent simulations based on the aforementioned experimental loading procedure. The unpoled specimen is subjected to incremental electrical load up to the saturation value, say 2.0 (MV m⁻¹), and unloaded to zero electric field, which gives the poled specimen a remanent polarization and strain. Subsequently, the compressive stress is applied

incrementally up to -75 (MPa); refer to figure 4(a)-I, which causes a partial mechanical depolarization response. At this stage, the applied uniaxial stress is kept constant and cyclic electric field loading is applied on the same specimen to obtain the ferroelectric response. These simulations are repeated for three different values of mechanical stress (-150, -225, -300 (MPa)).

The macroscopic coercive electric field, which determines the threshold for domain switching, decreases for increasing compressive stress; see figures 4(b) and (c). The main reason for this behavior stems from the fact that the underlying types of domain switching, namely 90° and 180° switching for the problem at hand, are differently activated under coupled loading conditions. The second major influence of the coupled electromechanical loading is the reduction in remanent and saturation polarization values of macroscopic electric displacement versus electric field curve. The slope of the loops at zero electrical field, which can be regarded as the permittivity, decreases when the magnitude of the compressive stress increases. Similarly, the area encircled by the hysteresis decreases with the increase of compressive stress as well. In addition, 4(b) and (c) clearly monitor that both the hysteresis as well as the butterfly curves 'flatten' with increasing compressive stresses. Considering the butterfly

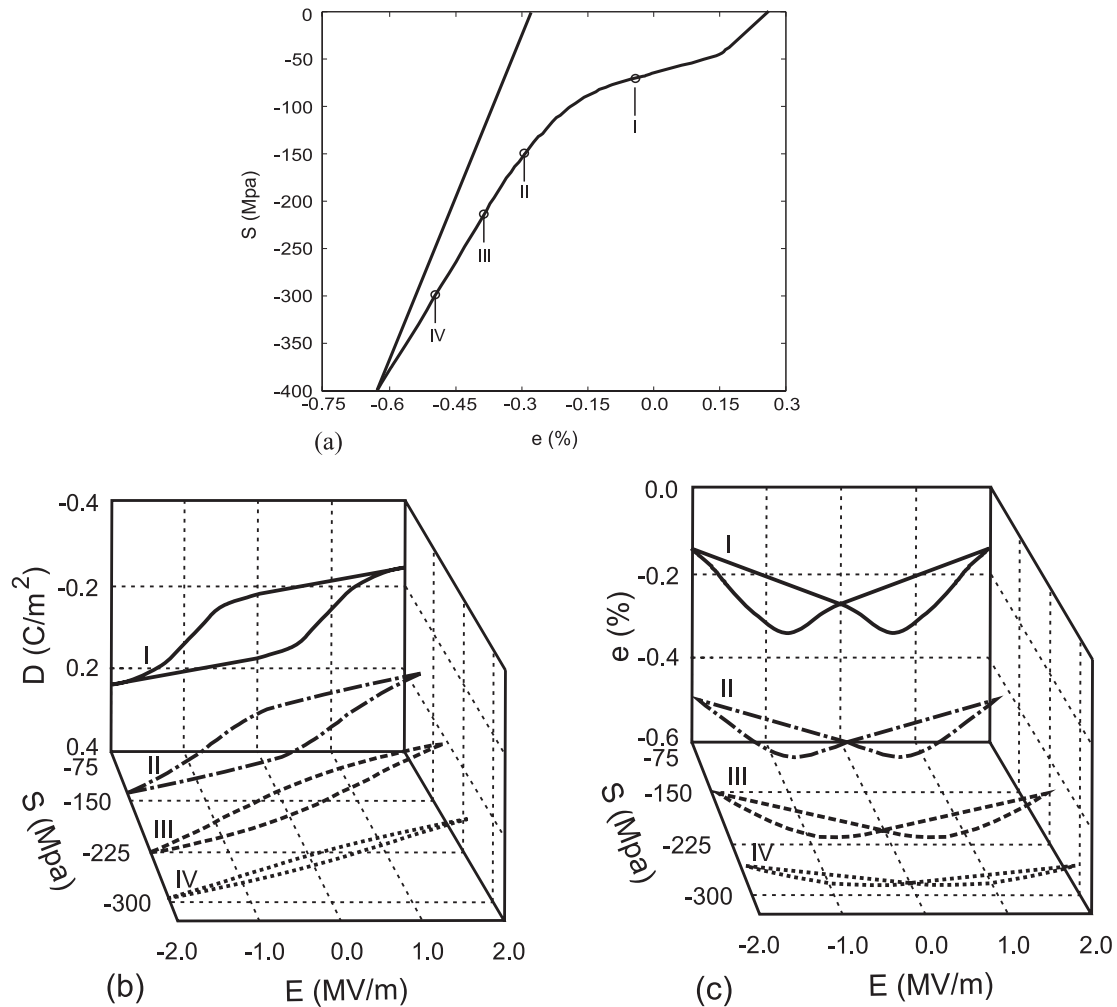


Figure 4. Hysteresis and butterfly curves are run at the various constant stress levels (I–IV) in a prepoled specimen (a); the resulting hysteresis and butterfly curves are subjected to uniaxial cyclic electric loading at different stresses ((b) and (c)).

curve, the longitudinal strain gradually becomes negative when the compressive stress becomes larger. The range of the strain variation becomes smaller and smaller as the magnitude of compressive stress increases. This means that the domain switching becomes more difficult under a larger magnitude of compressive stress together with electrical loading. At very high stress level, say at -300 (MPa), the electric field is not able to totally overcome the applied stress and there is very little strain. There is still, however, a noticeable component of polarization switching, though it is very small.

6.4. Uniaxial ferroelastic response under constant electric field

Another attempt has been made in simulation in which the unpoled specimen is subjected to incremental electrical load up to the saturation value, say 2.0 (MV m^{-1}), and unloaded to a certain value and maintained thereafter. Subsequently, the compressive stress is applied on the same specimen incrementally up to the saturation value and unloaded to zero stress in order to obtain the ferroelastic response; refer to figure 5(a). These simulations are repeated for four different values of electric field ($1.5, 1.0, 0.5, 0.0$ (MV m^{-1})).

The macroscopic coercive stress, which determines the threshold for domain switching, increases on increasing the electric field. Figures 5(b) and (c) show that, for the case of zero electric field, the compressive loading and unloading induces significant domain switching, which renders unrecovered remanent polarization and strain. In particular, under zero electric field, 90° domain switching and depolarization occurs when the compressive loading stress exceeds a critical threshold -75 (MPa) and during unloading, there is a very little re-polarization. It is further noted that the unrecovered polarization and hysteresis reduces with increasing magnitude of the constant electric field, implying that the electric field hampers the domain switching during the compressive loading in figure 5(c). The same behavior of decreased hysteresis on increasing the electric field has also been observed in figure 5(b) for the strain–stress curves. Since the constant electric field is in the same direction as that of the polarization, it in effect enforces the polarization and makes depolarization difficult during the mechanical loading–unloading cycle.

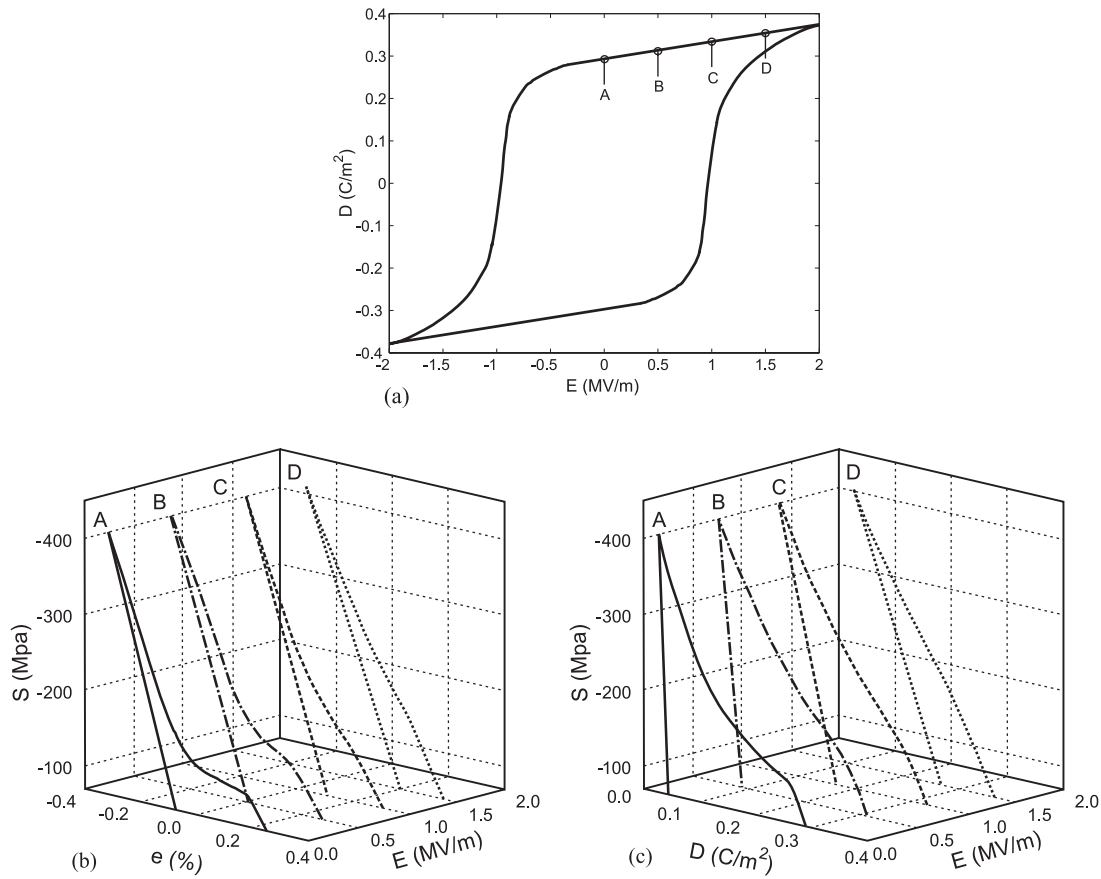


Figure 5. Stress versus strain and electric displacement curves are run at the various constant electric field levels (A–E) in a prepoled specimen (a); the resulting stress versus strain and electric displacement curves subjected to uniaxial mechanical loading at different fields ((b) and (c)).

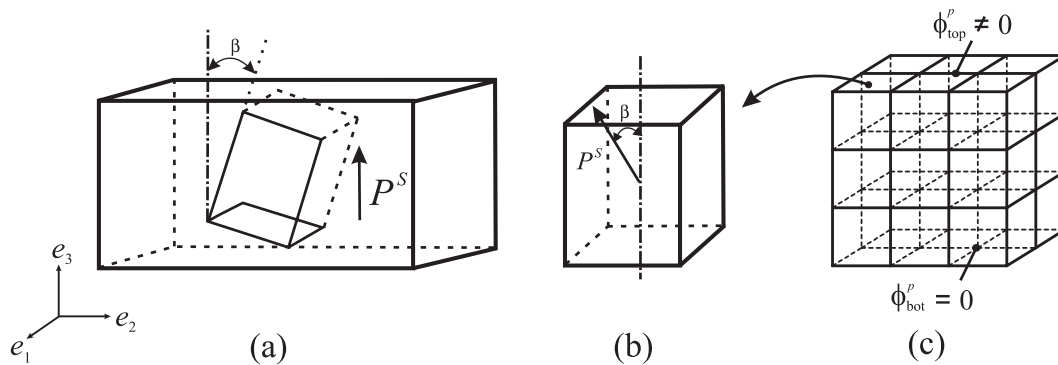


Figure 6. Experimental set-up for multiaxial loading by Huber and Fleck [13] ((a), (b)); finite element discretization and illustration of the applied boundary conditions (c).

6.5. Multiaxial electrical loading

Multiaxial electrical loading tests were performed by Huber and Fleck [13] to investigate the nonlinear ferroelectric response. The experiment started with an unpoled specimen and was then poled at room temperature by applying an electric field of maximum strength $2.0 \text{ (MV m}^{-1}\text{)}$. As shown in figure 6(a), rectangular blocks of uniform size were cut from the large parent specimen with their long axes inclined at a set of angles (from 0° to 180° , in steps of 45°) to the initial poling (remanent polarization) direction. The

multiaxial loading simulations are performed based on the experimental procedure, in which the poled test specimen is then subjected to electrical loading of increasing electric field up to $2.0 \text{ (MV m}^{-1}\text{)}$. The developed finite element formulation in the previous sections is used to simulate such a ferroelectric response. The discretization and the applied boundary conditions are illustrated in figure 6(c). Figure 7 shows the change in electric displacement and change in the total strain (3-axis) versus applied electric field (3-axis) for a selection of specimens at $\beta = 0^\circ; 45^\circ; 90^\circ; 135^\circ$ and 180° . Considering the case of $\beta = 0^\circ$, the direction of the applied

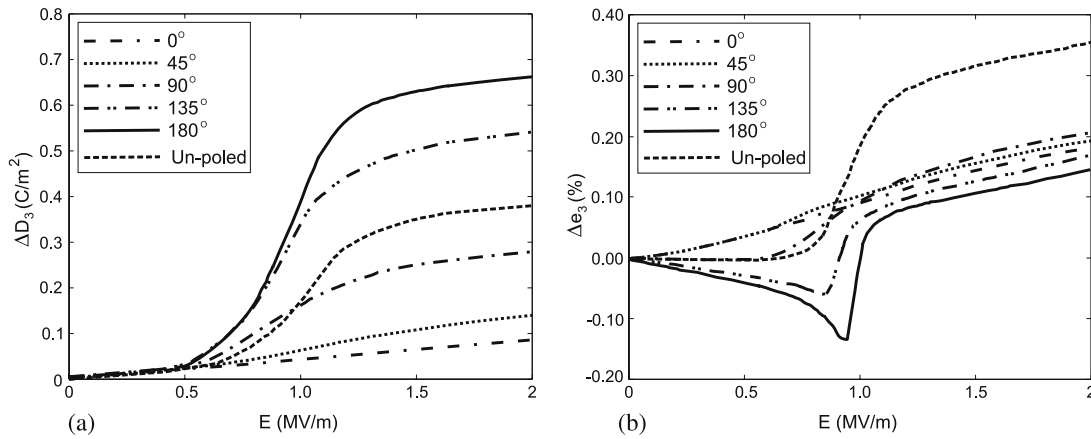


Figure 7. Electric displacement and strain responses (3-axis)—multiaxial electrical loading.

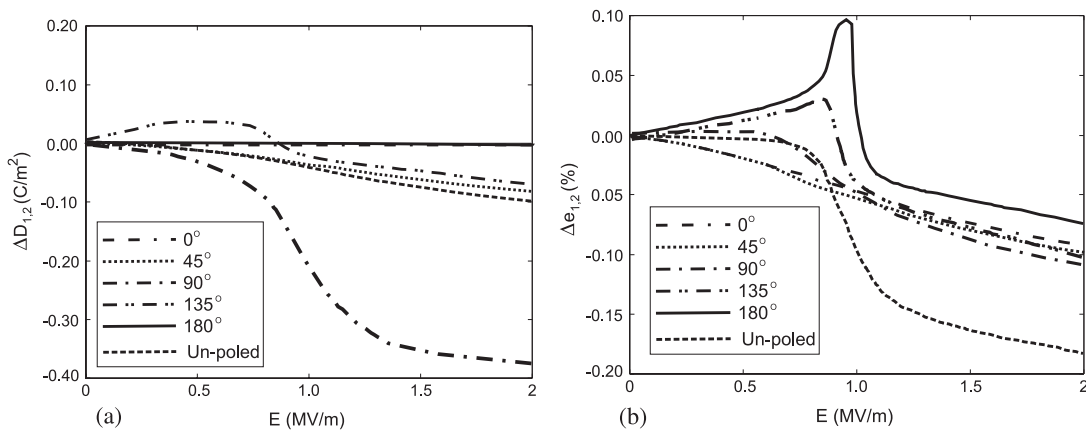


Figure 8. Electric displacement and strain responses (1- and 2-axis)—multiaxial electrical loading.

electric field is parallel to the initial poling direction. The predicted response is almost linear in the whole course of the electric displacement and strain versus electric field curves. This indicates that no switching occurs, since domains are already oriented in the direction of electric field and/or domain orientations have been saturated by the original or initial poling itself. As the angle (β) between the remanent polarization and the loading electric field increases, the simulated response changes nonlinearly in the electric displacement, and the strain due to ferroelectric domain switching becomes more and more pronounced. Since the direction of domain orientation of the polycrystals due to initial poling is different from the current loading directions, the domains which are required to reorient in line with the present applied loading is greater for higher angles of β , and thus renders an increase in nonlinear behavior. Concerning the specimen with $\beta = 180^\circ$, the applied electric field is anti-parallel to the initial poling direction. The observed results have the greatest nonlinearity in the displacement and strain curves, since the existing remanent polarization should be completely reversed. For the $\beta = 180^\circ$ case, the strain versus electric field curve shows that the initial strains are negative and then become positive, which gives an idea that the 180° domain switching is achieved by two consequent 90° switching. Figure 8 shows the change in electric displacement

and change in the total strain (1- and 2-axis) versus applied electric field (3-axis) for a selection of specimens at $\beta = 0^\circ; 45^\circ; 90^\circ; 135^\circ$ and 180° .

6.6. Multiaxial mechanical loading

Based on the multiaxial electrical loading test mentioned in the previous subsection, we performed the numerical simulation under multiaxial pure mechanical loading to investigate the ferroelastic response. Figure 9 shows the change in total strain and change in the electric displacement versus applied stress field for a selection of specimens at $\beta = 0^\circ; 45^\circ; 90^\circ; 135^\circ$ and 180° . Considering the case of $\beta = 0^\circ, 180^\circ$, the direction of the applied compressive stress is parallel to the initial poling direction. The observed results have the greatest nonlinearity in the strain and displacement curves, since the existing poled domains are subjected to compressive loading and 90° switching occurs. For the angle ($\beta = 90^\circ$), the predicted response is almost linear in the whole course of the strain and electric displacement versus stress curves, indicating that no switching occurs, since domains are already oriented perpendicular to the loading direction. Concerning the specimen with $\beta = 45, 135^\circ$, the simulated response shows some nonlinearity in the strain and displacement due

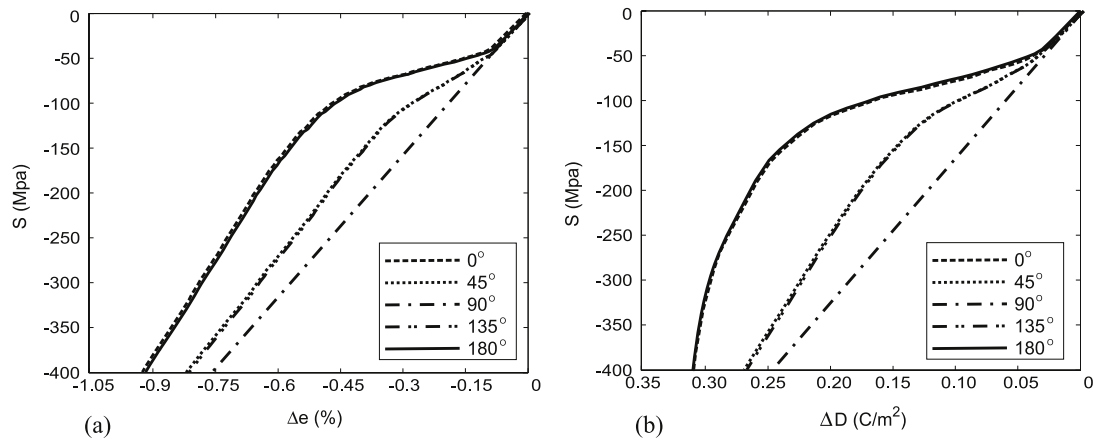


Figure 9. Strain and electric displacement responses (3-axis)—multiaxial mechanical loading.

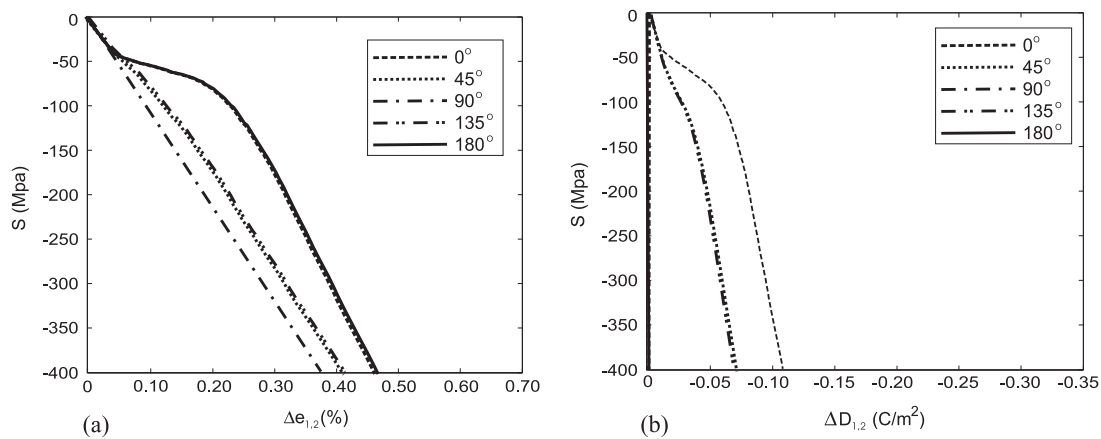


Figure 10. Strain and electric displacement responses (1- and 2-axis)—multiaxial mechanical loading.

to restricted domain switchings occurred. Figure 10 shows change in the total strain and change in electric displacement (1- and 2-axis) versus applied stress (3-axis) for a selection of specimens at $\beta = 0; 45; 90; 135$ and 180° .

7. Summary

A three-dimensional micromechanical model has been developed to simulate the nonlinear behavior of polycrystalline ferroelectrics. Considering that the virgin state of these materials is commonly unpoled, initial orientations of polarization vectors are randomly generated. The onset of domain switching was introduced by means of a thermodynamically consistent dissipation threshold. The adopted model for ferroelectric materials is embedded into a finite element formulation, with each finite element representing an individual grain. The grain boundary effects are incorporated by means of an additional term in the switching criterion so that switching now depends on the constraints imposed by the surrounding grains. The material constants such as elastic, dielectric and piezoelectric constants are updated according to the switching process. Numerical tests show that the simulated hysteresis and butterfly loops are in qualitative agreement with experimental observations. In

particular, the smooth transition of switching initiation near the coercive electric and mechanical fields is observed upon introducing this effect.

Acknowledgments

AA would like to acknowledge the support by the Department of Science and Technology (DST), India under the SERC—Fast Track scheme through grant no. SR/FT/ET-001/2009. The authors wish to acknowledge the useful discussions they had with Mr K Jayabal during the development of the model.

References

- [1] Allik H and Hughes T J R 1970 Finite element method for piezoelectric vibration *Int. J. Numer. Methods Eng.* **2** 151–7
- [2] Arockiarajan A, Menzel A, Delibas B and Seemann W 2006 Computational modeling of rate-dependent domain switching in piezoelectric materials *Eur. J. Mech. A* **25** 950–64
- [3] Arockiarajan A, Menzel A, Delibas B and Seemann W 2006 Micromechanical modeling of switching effects in piezoelectric materials—a robust coupled finite element approach *J. Intell. Mater. Syst. Struct.* **18** 983–99

- [4] Bassiouny E, Ghaleb A and Maugin G 1998 Thermodynamical formulation for coupled electromechanical hysteresis effects I. Basic equations *Int. J. Eng. Sci.* **26** 1279–95
- [5] Chaplya P M and Carman G P 2001 Dielectric and piezoelectric response of lead zirconate-lead titanate at high electric and mechanical loads in terms of non-180° domain wall motion *J. Appl. Phys.* **90** 5278–86
- [6] Chen W and Lynch C S 1998 A micro-electro-mechanical model for polarization switching of ferroelectric materials *Acta Mater.* **46** 5303–11
- [7] Cook R D 1982 Loubignac's iterative method in finite element elastostatics *Int. J. Numer. Methods Eng.* **18** 67–75
- [8] Elhadrouz M, Zineb T B and Patoor E 2005 Constitutive law for ferroelastic and ferroelectric piezoceramics *J. Intell. Mater. Syst. Struct.* **16** 221–36
- [9] Gabbert U, Berger H, Köppe H and Cao X 2000 On modelling and analysis of piezoelectric smart structures by the finite element method *Int. J. Appl. Mech. Eng.* **5** 127–42
- [10] Gaudenzi P and Bathe K J 1995 An iterative finite element procedure for the analysis of piezoelectric continua *J. Intell. Mater. Syst. Struct.* **6** 266–73
- [11] Goldstein H, Poole C and Safko J P 2002 *Classical Mechanics* 3rd edn (New York: Addison-Wesley)
- [12] Huber J E, Fleck N A, Landis C M and McMeeking R M 1999 A constitutive model for ferroelectric polycrystals *J. Mech. Phys. Solids* **47** 1663–97
- [13] Huber J E and Fleck N A 2001 Multi-axial electrical switching of a ferroelectric: theory versus experiment *J. Mech. Phys. Solids* **49** 785–811
- [14] Huber J E and Fleck N A 2004 Ferroelectric switching: a micromechanics model versus measured behaviour *Eur. J. Mech. A* **23** 203–17
- [15] Huber J E 2005 Micromechanical modeling of ferroelectrics *Curr. Opin. Solid State Mater. Sci.* **9** 100–6
- [16] Hwang S C, Lynch C S and McMeeking R M 1995 Ferroelectric/ferroelastic interactions and a polarization switching model *Acta Metall. Mater.* **43** 2073–84
- [17] Hwang S C and Waser R 2000 Study of electrical and mechanical contribution to switching in ferroelectric and ferroelastic polycrystals *Acta Mater.* **48** 3271–82
- [18] Haug A, Onck P R and Van der Giessen E 2007 Development of inter- and intragranular stresses during switching of ferroelectric polycrystals *Int. J. Solids Struct.* **44** 2066–78
- [19] Kamlah M and Jiang Q 1999 A constitutive model for ferroelectric PZT ceramics under uniaxial loading *Smart Mater. Struct.* **8** 441–59
- [20] Kamlah M and Bohle U 2001 Finite element analysis of piezoceramic components taking into account ferroelectric hysteresis behaviour *Int. J. Solids Struct.* **38** 605–33
- [21] Kamlah M 2001 Ferroelectric and ferroelastic piezoceramics-modeling and electromechanical hysteresis phenomena *Continuum Mech. Thermodyn.* **13** 219–68
- [22] Kim S J and Jiang Q 2002 A finite element model for rate-dependent behavior of ferroelectric ceramics *Int. J. Solids Struct.* **39** 1015–30
- [23] Klinkel S 2006 A phenomenological constitutive model for ferroelastic and ferroelectric hysteresis effects in ferroelectric ceramics *Int. J. Solids Struct.* **43** 7197–222
- [24] Landis C M and McMeeking R M 2000 A phenomenological constitutive law for ferroelastic switching and a resulting asymptotic crack tip solution *J. Intell. Mater. Syst. Struct.* **10** 155–63
- [25] Landis C M 2002 Fully coupled, multi-axial, symmetric constitutive laws for polycrystalline ferroelectric ceramics *J. Mech. Phys. Solids* **50** 127–52
- [26] Landis C M 2004 Non-linear constitutive modeling of ferroelectrics *Curr. Opin. Solid State Mater. Sci.* **8** 59–69
- [27] Lynch C S 1996 The effect of uniaxial stress on the electro-mechanical response of 8/65/35 PLZT *Acta Mater.* **44** 4137–48
- [28] Menzel A, Arockiarajan A and Sivakumar S M 2008 Two models to simulate rate-dependent domain switching effects-application to ferroelastic polycrystalline ceramics *Smart Mater. Struct.* **17** 015026
- [29] Pathak A and McMeeking R M 2008 Three-dimensional finite element simulations of ferroelectric polycrystals under electrical and mechanical loading *J. Mech. Phys. Solids* **56** 663–83
- [30] Sateesh V L, Upadhyay C S and Venkatesan C 2008 Thermodynamic modeling of hysteresis effects in piezoceramics for application to smart structures *AIAA J.* **46** 280–4
- [31] Schröder J and Romanowski H C 2005 A thermodynamically consistent mesoscopic model for transversely isotropic ferroelectric ceramics in a coordinate-invariant setting *Arch. Appl. Mech.* **74** 863–77
- [32] Shieh J, Huber J E and Fleck N A 2003 An evaluation of switching criteria for ferroelectrics under stress and electric field *Acta Mater.* **51** 6123–37
- [33] Smith R C *Smart Material Systems—Model Development* (Philadelphia: SIAM)
- [34] Veland D and Chen Y-H 2000 Random-field model for ferroelectric domain dynamics and polarisation reversal *J. Appl. Phys.* **88** 6696–707
- [35] Zhang Z K, Fang D N and Soh A K 2006 A new criterion for domain-switching in ferroelectric materials *Mech. Mater.* **38** 25–32
- [36] Zhou D, Kamlah M and Munz D 2005 Effects of uniaxial prestress on the ferroelectric hysteretic response of soft PZT *J. Eur. Ceram. Soc.* **25** 425–43
- [37] Zhou D, Kamlah M and Munz D 2005 Effects of bias electric fields on the non-linear ferroelastic behavior of soft lead zirconate titanate piezoceramics *J. Am. Ceram. Soc.* **88** 867–74